

# SCIENTIFIC REPORTS

OPEN

## Wide-Range Probing of Dzyaloshinskii–Moriya Interaction

Duck-Ho Kim<sup>1,†</sup>, Sang-Cheol Yoo<sup>1,2</sup>, Dae-Yun Kim<sup>1</sup>, Byoung-Chul Min<sup>2</sup> & Sug-Bong Choe<sup>1</sup>

Received: 19 October 2016

Accepted: 28 February 2017

Published: 31 March 2017

The Dzyaloshinskii–Moriya interaction (DMI) in magnetic objects is of enormous interest, because it generates built-in chirality of magnetic domain walls (DWs) and topologically protected skyrmions, leading to efficient motion driven by spin–orbit torques. Because of its importance for both potential applications and fundamental research, many experimental efforts have been devoted to DMI investigation. However, current experimental probing techniques cover only limited ranges of the DMI strength and have specific sample requirements. Thus, there are no versatile methods to quantify DMI over a wide range of values. Here, we present such an experimental scheme, which is based on the angular dependence of asymmetric DW motion. This method can be used to determine values of DMI much larger than the maximum strength of the external magnetic field strength, which demonstrates that various DMI strengths can be quantified with a single measurement setup. This scheme may thus prove essential to DMI-related emerging fields in nanotechnology.

The Dzyaloshinskii–Moriya interaction (DMI) is an antisymmetric exchange interaction that occurs at interfaces between ferromagnetic and heavy metal layers with large spin–orbit coupling<sup>1–3</sup>. In magnetic systems, DMI generates chiral spin textures such as Néel domain walls (DWs)<sup>4–7</sup> and magnetic skyrmions<sup>8–10</sup>. Because these chiral spin textures promise several potential applications<sup>4,7,8</sup>, it is crucial to quantify the strength of the DMI both to better understand its physical origin and for the technical optimization of ferromagnetic materials.

Several experimental schemes have been proposed to measure the DMI strength<sup>5,6,11–15</sup>. Using an optical microscope, it has been developed a method to estimate it based on the field-driven asymmetric DW speed with respect to an in-plane magnetic field<sup>11,16,17</sup> and the current-driven asymmetric DW speed<sup>5,6</sup>. Moon *et al.*<sup>12</sup> suggested another approach based on the frequency nonreciprocity, which provides a way to measure the DMI constant. Other measurement schemes relying on the nonreciprocal propagation of spin waves were demonstrated using Brillouin light scattering (BLS)<sup>18–20</sup> and inductive ferromagnetic resonance (FMR)<sup>21</sup>. All these techniques are applicable to different ranges of DMI strength and have different sample requirements.

The optical microscopy technique<sup>11,16,17</sup> based on asymmetric DW speed provides an easy and direct way to measure DMI-induced effective magnetic fields. However, its measurement range is limited by the maximum strength of the external in-plane magnetic field, which in turn is fundamentally constrained by the narrow space available inside the optical setup. Moreover, application of large external magnetic fields to the optical setup requires sophisticated care to prevent artifacts caused by stray fields from electromagnets as well as mechanical, optical, and thermal artifacts from such strong magnetic fields. In this study, we propose a way to overcome this field strength limit by utilizing DWs, inclined at an angle with respect to the direction of the in-plane magnetic field.

### Results

**DW energy model for a DW at an angle  $\theta$ .** The inset in Fig. 1 shows the case where a DW is placed at an angle  $\theta$  with respect to an in-plane magnetic field,  $H_x$ . The DW energy density  $\sigma_{\text{DW}}$  can be expressed as a function of  $H_x$  and the angle  $\psi$  between the magnetization direction and the normal to the DW<sup>3,11</sup>:

$$\sigma_{\text{DW}}(H_x, \psi) = \sigma_0 + 2\lambda K_D \cos^2 \psi - \pi \lambda M_S [(H_x \cos \theta + H_{\text{DMI}}) \cos \psi + H_x \sin \theta \sin \psi], \quad (1)$$

where  $\sigma_0$  is the Bloch-type DW energy density,  $\lambda$  is the DW width,  $K_D$  is the DW-anisotropy energy density,  $M_S$  is the saturation magnetization, and  $H_{\text{DMI}}$  is the DMI-induced effective magnetic field in the direction normal to the DW. The second term in the right-hand side of the equation corresponds to the DW-anisotropy energy and the

<sup>1</sup>Department of Physics and Institute of Applied Physics, Seoul National University, Seoul, 08826, Republic of Korea.

<sup>2</sup>Center for Spintronics, Korea Institute of Science and Technology, Seoul, 02792, Republic of Korea. <sup>†</sup>Present address: Institute for Chemical Research, Kyoto University, Uji, Kyoto, 611-0011 Japan. Correspondence and requests for materials should be addressed to S.-B.C. (email: sugbong@snu.ac.kr)

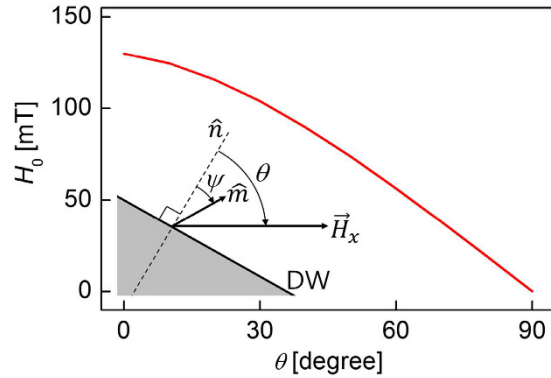


**Figure 1.** Plot of  $H_0$  as a function of  $\theta$ . The Red solid line is calculated by using Eq. (4). The inset is an schematic illustration of the measurement geometry.

third term to the Zeeman energy, including the DMI as an effective magnetic field. Note that Eq. (1) is identical to the Stoner–Wohlfarth equation<sup>22</sup> for torque magnetometry with an additional unidirectional bias from  $H_{\text{DMI}}$ .

For a given  $H_x$ , the equilibrium angle  $\psi_{\text{eq}}$  can be obtained by the minimization condition  $\partial\sigma_{\text{DW}}/\partial\psi|_{\psi_{\text{eq}}} = 0$ . Moreover, a numerical analysis of Eq. (1) shows that  $\sigma_{\text{DW}}$  has a maximum at  $H_x = H_0$ , where  $H_0$  can be obtained from the maximization condition  $\partial\sigma_{\text{DW}}/\partial H_x|_{H_0} = 0$ . By solving these minimization and maximization conditions simultaneously, one can readily obtain two coupled equations:

$$4K_{\text{D}} \cos\psi_{\text{eq}} \sin\psi_{\text{eq}} - \pi M_{\text{S}}[(H_0 \cos\theta + H_{\text{DMI}})\sin\psi_{\text{eq}} - H_0 \sin\theta \cos\psi_{\text{eq}}] = 0, \quad (2)$$

$$\cos\theta \cos\psi_{\text{eq}} + \sin\theta \sin\psi_{\text{eq}} = 0. \quad (3)$$

Equation (3) is identical to the relation  $\psi_{\text{eq}} = \theta \mp \pi/2$ , which implies that the DW magnetization stays perpendicular to the direction of  $H_0$ . Inserting this value of  $\psi_{\text{eq}}$  into Eq. (2), it can be rewritten as

$$H_0 = (\pm H_{\text{K}} \sin\theta - H_{\text{DMI}})\cos\theta, \quad (4)$$

where  $H_{\text{K}} (\equiv 4K_{\text{D}}/\pi M_{\text{S}})$  is the DW-anisotropy field, which usually is small. Hence, in practice, the sign of the first term on the right-hand side of Eq. (4) coincides with that of  $H_{\text{DMI}}$ , i.e., a plus sign for a positive  $H_{\text{DMI}}$  and a minus sign for a negative  $H_{\text{DMI}}$ . Note that the well-known relation  $H_0 = -H_{\text{DMI}}$ <sup>11,16,17</sup> can be restored in the limit  $\theta \rightarrow 0$ . Figure 1 plots the value of  $H_0(\theta)$  obtained from Eq. (4). This plot shows that  $H_0$  has the clear angle dependence.

Equation (4) contains the key idea of this study: one can significantly reduce the value of  $H_0$  by increasing  $\theta$ . With this scheme, the magnitude of  $H_0$  can be adjusted down to a small experimental range  $H_{\text{range}}$  of the external magnetic field, which allows one to measure a large  $H_{\text{DMI}}$  without upgrading the electromagnet. For example, by tilting the DWs up to about  $80^\circ$ , one can measure  $H_{\text{DMI}}$  up to 1 T using an electromagnet with  $H_{\text{range}} \sim 200$  mT, which is easily achieved in conventional optical setups<sup>23</sup>. It is also worth noting that by using this approach we can prevent a number of artifacts caused by large magnetic fields, such as mechanical instability produced by the induced magnetic moment in the optical setup, magneto-optical effects in the objective lens, and large Joule heating caused by the huge currents passing through the electromagnet.

**Verification of  $\theta$ -dependence in Pt/Co/ $\text{AlO}_x$  films.** To verify the feasibility of the present scheme, it was applied to ferromagnetic Pt/Co/ $\text{AlO}_x$  films, for which  $H_{\text{DMI}}$  is slightly smaller than  $H_{\text{range}}$ . The procedure to measure  $H_0$  closely follows ref. 11, except for the initially tilted DWs. The tilted DWs were generated using a thermomagnetic writing technique<sup>7,24,25</sup> (see Methods). The images in the right panel of Fig. 2 show the displacements of the DWs for various values of  $\theta$  with respect to the direction of in-plane magnetic field  $H_x$  ( $=120$  mT) under the application of a fixed out-of-plane magnetic field  $H_z$  ( $=5.5$  mT) bias. Each image was obtained by adding several images, sequentially acquired during the DW displacement with a constant time step ( $=500$  ms). Thus, each image simultaneously shows several DWs moving from brighter to darker interfaces as time goes by. One can then measure the DW speed  $v$  for each image. The plots in the left panel of Fig. 2 show the normalized DW speed  $v/v_{\text{min}}$  in the direction normal to the DW as a function of  $H_x$  (in creep regime), where  $v_{\text{min}}$  is the apparent minimum of  $v$ . It can be seen that  $v(H_x)$  is symmetric under inversion with respect to  $H_0^*$  as shown in each plot. Here,  $H_0^*$  indicates the inversion symmetry axis where  $v$  has a minimum. According to ref. 11,  $v$  follows the creep relation  $\ln[v(H_x)/v_0] \propto -[\sigma_{\text{DW}}(H_x)]^{1/4}$ , where  $v_0$  is the characteristic speed. In the case of clear inversion symmetry with a constant  $v_0$ , the experimental  $H_0^*$  exactly matches  $H_0$ , and thus, we will denote  $H_0^*$  by  $H_0$  hereafter.

Figure 3a plots the measured  $H_0$  as a function of  $\theta$ . The red solid line shows the best fit to Eq. (4). The good agreement between the data and the fitting curve supports again the validity of the equation. The best-fit  $H_{\text{DMI}}$  ( $= -132 \pm 3$  mT) matches well the experimental value ( $= -134 \pm 6$  mT) measured at  $\theta = 0$ . Moreover, the best-fit value of  $H_{\text{K}}$  ( $= -18 \pm 5$  mT) falls within the range of previous experimental reports<sup>11,26,27</sup>. The value of  $H_{\text{K}}$  can be

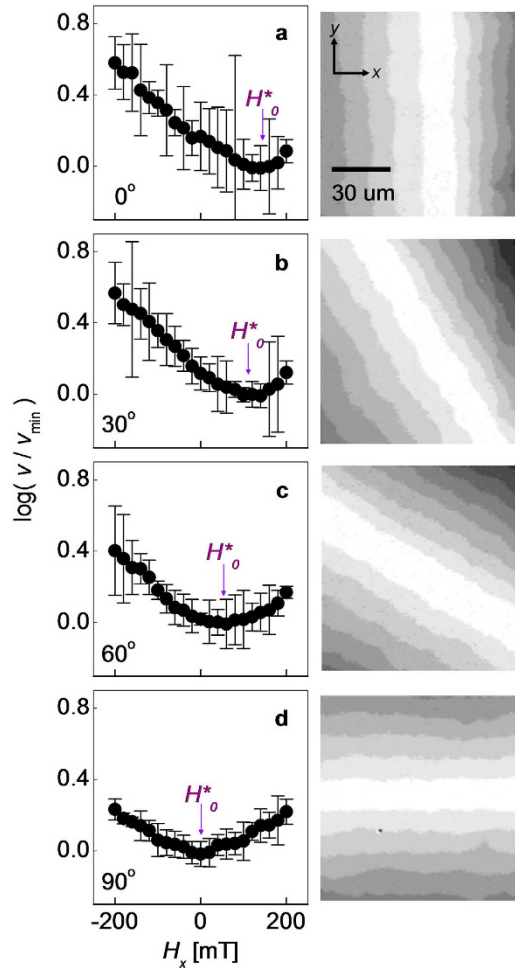


**Figure 2.** Plot of  $v/v_{\min}$  as a function of  $H_x$  in a Pt/Co/AlO<sub>x</sub> film, for fixed  $H_z = 5.5$  mT and under various values of  $\theta$ . (a) 0° (b) 30° (c) 60°, and (d) 90°. The displacement of the DWs at each angle is driven by the external magnetic fields.

alternatively measured through independent measurements<sup>11,26,27</sup> or estimated using the relation  $H_K \cong (4 \ln 2 / \pi^2) M_s t_f / \lambda$ <sup>28,29</sup>, where  $t_f$  is the thickness of the magnetic layer.

**Application of present scheme to Pt/Co/AlO<sub>x</sub> and Pt/Co/MgO films.** To reproduce a situation in which  $H_{\text{range}}$  is limited ( $< 50$  mT), the fit was also performed only for the data (box in the plot) with large  $\theta$  ( $\geq 70^\circ$ ) as shown in Fig. 3b. The blue solid line indicates the best fit to Eq. (4), using the fixed value of  $H_K$  obtained from Fig. 3a. This approach gives the best-fit value  $H_{\text{DMI}} (= -138 \pm 12$  mT), which again matches the previous values within the experimental accuracy. It is therefore demonstrated that the present approach enables one to measure large  $H_{\text{DMI}}$  in an experiment with limited  $H_{\text{range}}$ . Note that the determined  $H_{\text{DMI}}$  is more than twice larger than  $H_{\text{range}}$ .

Because the fit in Fig. 3b was performed with a fixed  $H_K$ , now we examine the effect of the inaccuracy  $\delta H_K$  on  $H_K$ . The blue dotted lines in Fig. 3b are the best fits when  $\delta H_K = \pm 10$  mT. The error  $\delta H_{\text{DMI}}$  is found to be slightly smaller than  $\delta H_K$ , as expected from the relation  $\delta H_{\text{DMI}} = \delta H_K \sin \theta$  deduced from Eq. (4). Because  $H_K$  is commonly within the range of a few tens of mT<sup>11,26–28,30</sup>,  $\delta H_K$  typically will not exceed about  $\pm 10$  mT, and thus one can confirm that the error induced by  $\delta H_K$  error is not significantly large as compared to other experimental errors. Moreover, this error becomes negligible in practical cases because the present approach is designed for the determination of large  $H_{\text{DMI}}$  ( $\gg \delta H_K$ ), significantly beyond the experimental  $H_{\text{range}}$ .

Finally, the present scheme was applied to Pt/Co/MgO films, which exhibit DMI larger than  $H_{\text{range}}$ . Figure 4a shows  $v$  as a function of  $H_x$  for  $\theta = 0$ . From this plot, it is apparent that the inversion symmetry axis  $H_0$  lies far beyond the experimental  $H_{\text{range}}$  (i.e.,  $H_0 \gg 200$  mT), and thus conventional optical schemes cannot be used to quantify  $H_{\text{DMI}}$ . However, by applying the present method, Fig. 4b shows the measured  $H_0$  with respect to  $\theta$  for large  $\theta$  ( $\geq 80^\circ$ ). The black box in the figure indicates the measurable window for  $H_{\text{range}}$  in the present setup. The best fit (blue solid line) of  $H_K$  ( $= -30 \pm 5$  mT) indicates that  $H_{\text{DMI}} = -483 \pm 10$  mT, which is more than twice larger than  $H_{\text{range}}$ . The sign and magnitude are in good agreement with previously reported results<sup>21</sup>. The blue dotted lines in Fig. 4b are the best fits for the cases with  $\delta H_K = \pm 10$  mT, and thus it is clearly demonstrated that the error becomes negligible in this case.

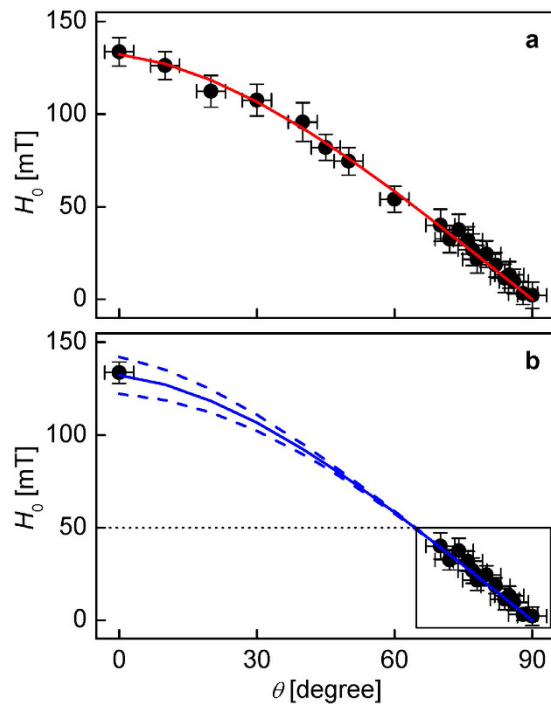


**Figure 3.** Plot of the measured  $H_0$  as a function of  $\theta$  in a Pt/Co/AlO<sub>x</sub> film. (a) Data collected for large  $\theta$  range (from 0° to 90°). The red solid line shows the best fit to Eq. (4). (b) Data collected within a small  $\theta$  range (from 70° to 90°). The blue solid line represents the best fit to Eq. (4) with the value of  $H_K$  fixed. The blue dotted lines in (b) are the best fits for the cases with  $\delta H_K = \pm 10$  mT.

## Discussion

Additional asymmetry from chiral damping<sup>31</sup> or asymmetric DW width variation<sup>28</sup> may cause a shift  $\delta H_0$  in  $H_0$ . However, because the asymmetric slope in  $v$  caused by these phenomena appears only during chirality variation occurring within the range of  $\pm H_K$ ,  $|\delta H_0|$  is essentially smaller than  $|H_K|$ . Therefore,  $\delta H_0$ -induced errors are negligible again in practice for large  $H_{DMI}$  determination.

In conclusion, we proposed a scheme to measure  $H_{DMI}$  over a wide range of values, overcoming the limitations caused by the small strength ( $H_{range}$ ) of the external magnetic fields typically used in experiments. By measuring the angular dependence of asymmetric DW motion, we found that  $H_0$  is strongly correlated with  $\theta$ , which means that large DMI can be quantified in a robust manner by setting large values of  $\theta$ . The feasibility of the present approach is experimentally demonstrated for various DMI strengths using ferromagnetic Pt/Co/AlO<sub>x</sub> and Pt/Co/MgO films. The errors caused by additional asymmetry and inaccuracy of  $H_K$  were found to be negligible in practice for large  $H_{DMI}$  determination. The present scheme enhances the experimental range of optical measurement techniques without the need upgrade electromagnets. Our findings represent a novel and straightforward way to explore materials and systems with large DMI, and thus surmounts the key obstacle to design new devices in which the DMI is tailored to achieve for topological stability and efficient manipulation, as required for next-generation nanotechnology.

## Methods

**Sample preparation.** For this study, we prepared 5.0-nm Ta/3.0-nm Pt/0.6-nm Co/1.6-nm AlO<sub>x</sub> and 5.0-nm Ta/3.0-nm Pt/0.6-nm Co/2.0-nm MgO films, which were deposited on a Si wafer with a 100 nm SiO<sub>2</sub> layer by dc magnetron sputtering<sup>23</sup>. To enhance the sharpness of the layer interfaces, we set a small deposition rate ( $=0.25$  Å/s) through adjustment of the Ar sputtering pressure ( $\sim 2$  mTorr) and power ( $\sim 10$  W). All the films exhibited strong perpendicular magnetic anisotropy and circular domain expansion with weak pinning strength.

**Thermomagnetic writing of tilted domain walls.** To create tilted DWs, we adopted a thermomagnetic writing technique<sup>7,24,25</sup>. The film was first saturated by a magnetic field ( $= -10$  mT) and then, a laser beam ( $= 75$  mW) was focused onto a small spot ( $5$   $\mu$ m in diameter) of the film under a reversed magnetic field ( $= 3.3$  mT) smaller than the coercive field ( $= 8$  mT). At this instant, the sample stage was moved along a desired direction, resulting in formation of a tilted straight DW. Alternatively, tilted DWs can be obtained from small arcs of larger circular domains.

**Experimental setup and measurement.** The magnetic domain images were acquired using a magneto-optical Kerr effect (MOKE) microscope equipped with a charge-coupled device (CCD) camera. To apply the magnetic field onto the films, two electromagnets were attached to the sample stage. One of them was used to produce an in-plane magnetic field bias  $H_x$  up to 200 mT, whereas the other created an out-of-plane

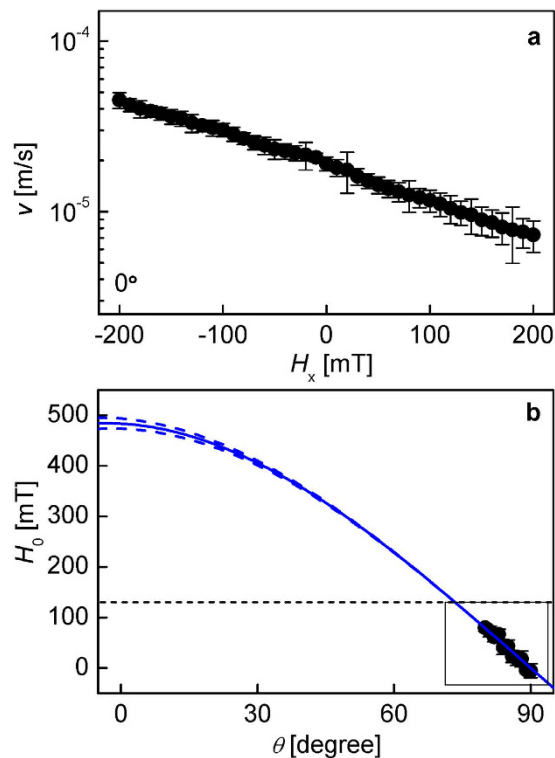


**Figure 4. DMI determination in Pt/Co/MgO film.** (a) Plot of the measured  $v$  as a function of the in-plane field  $H_x$ , for fixed  $H_z = 20$  mT, at  $\theta = 0$ . (b) Plot of the measured  $H_0$  as a function of  $\theta$ , for values of  $\theta$  between  $80^\circ$  and  $90^\circ$ . The blue solid line shows the best fit to Eq. (4) and the blue dotted lines in (b) are the best fits for the cases with  $\delta H_k = \pm 10$  mT.

magnetic field  $H_z$  up to 35 mT. The possible effect from the small misalignment of the in-plane magnet as well as the ambient magnetic field is included in the  $H_z$  calibration, where this ambient magnetic field can be estimated by measuring the DW speed along right direction when  $+H_x$  is applied and the DW speed along left direction when  $-H_x$  is applied. This field difference between them is come from the small misalignment of the in-plane magnet. Using this system, the field-driven DW speed  $v$  was measured in the creep regime. To do so, a linear DW was initially placed at a tilted angle  $\theta$ , as shown in the inset of Fig. 1, and then the DW displacement in the normal direction of the DW was monitored by the MOKE microscope under application of constant  $H_z$  and/or  $H_x$ . The dependence of  $v$  on  $H_x$  exhibits asymmetries attributed to the variation of the DW energy density with  $H_x$ , and the DMI-induced effective field can be directly quantified at a local minimum<sup>11</sup>.

## References

- Dzyaloshinskii, I. E. Thermodynamic theory of weak ferromagnetism in antiferromagnetic substances. *Sov. Phys. JETP* **5**, 1259–12172 (1957).
- Moriya, T. Anisotropic superexchange interaction and weak ferromagnetism. *Phys. Rev.* **120**, 91–98 (1960).
- Thiaville, A., Rohart, S., Jué, É., Cros, V. & Fert, A. Dynamics of Dzyaloshinskii domain walls in ultrathin magnetic films. *Europhys. Lett.* **100**, 57002 (2012).
- Parkin, S. & Yang, S.-H. Memory on the racetrack. *Nature Nanotech.* **10**, 195–198 (2015).
- Ryu, K.-S., Thomas, L., Yang, S.-H. & Parkin, S. Chiral spin torque at magnetic domain walls. *Nature Nanotech.* **8**, 527–533 (2013).
- Yang, S.-H., Ryu, K.-S. & Parkin, S. Domain-wall velocities of up to  $750 \text{ m s}^{-1}$  driven by exchange-coupling torque in synthetic antiferromagnets. *Nature Nanotech.* **10**, 221–226 (2015).
- Moon, K.-W. *et al.* Magnetic bubblecade memory based on chiral domain walls. *Sci. Rep.* **5**, 9166 (2015).
- Fert, A., Cros, V. & Sampaio, J. Skyrmions on the track. *Nature Nanotech.* **8**, 152–156 (2013).
- Sampaio, J., Cros, V., Rohart, S., Thiaville, A. & Fert, A. Nucleation, stability and current-induced motion of isolated magnetic skyrmions in nanostructures. *Nature Nanotech.* **8**, 839–844 (2013).
- Jiang, W. *et al.* Blowing magnetic skyrmion bubbles. *Science* **349**, 283–286 (2015).
- Je, S.-G. *et al.* Asymmetric magnetic domain-wall motion by the Dzyaloshinskii–Moriya interaction. *Phys. Rev. B* **88**, 214401 (2013).
- Moon, J.-H. *et al.* Spin-wave propagation in the presence of interfacial Dzyaloshinskii–Moriya interaction. *Phys. Rev. B* **88**, 184404 (2013).
- Pizzini, S. *et al.* Chirality-induced asymmetric magnetic nucleation in Pt/Co/AlOx ultrathin microstructures. *Phys. Rev. Lett.* **113**, 047203 (2014).
- Han, D.-S. *et al.* Asymmetric hysteresis for probing Dzyaloshinskii–Moriya interaction. *Nano Lett.* **16**, 4438–4446 (2016).
- Dmitrienko, V. E. *et al.* Measuring the Dzyaloshinskii–Moriya interaction in a weak ferromagnet. *Nature Phys.* **10**, 202–206 (2014).
- Hrabec, A. *et al.* Measuring and tailoring the Dzyaloshinskii–Moriya interaction in perpendicularly magnetized thin films. *Phys. Rev. B* **90**, 020402(R) (2014).
- Kim, D.-H., Yoo, S.-C., Kim, D.-Y., Min, B.-C. & Choe, S.-B. Universality of Dzyaloshinskii–Moriya interaction effect over domain-wall creep and flow regimes. arXiv:1608.01762 (2016).

18. Belmeguenai, M. *et al.* Interfacial Dzyaloshinskii–Moriya interaction in perpendicularly magnetized Pt/Co/AlOx ultrathin films measured by Brillouin light spectroscopy. *Phys. Rev. B* **91**, 180405(R) (2015).
19. Cho, J. *et al.* Thickness dependence of the interfacial Dzyaloshinskii–Moriya interaction in inversion symmetry broken systems. *Nat. Commun.* **6**, 7635 (2015).
20. Nembach, H. T., Shaw, J. M., Weiler, M., Jué, E. & Silva, T. J. Linear relation between Heisenberg exchange and interfacial Dzyaloshinskii–Moriya interaction in metal films. *Nature Phys.* **11**, 825–829 (2015).
21. Lee, J.-M., Jang, C., Min, B.-C., Lee, K.-J. & Chang, J. All-electrical measurement of interfacial Dzyaloshinskii–Moriya interaction using collective spin-wave dynamics. *Nano Lett.* **16**, 62–67 (2016).
22. Chikazumi S. *Physics of Ferromagnetism* (2nd ed.) 495–498 (Oxford: Clarendon, 1997).
23. Kim, D.-H. *et al.* Maximizing domain-wall speed via magnetic anisotropy adjustment in Pt/Co/Pt films. *Appl. Phys. Lett.* **104**, 142410 (2014).
24. Moon, K.-W. *et al.* Distinct universality classes of domain wall roughness in two-dimensional Pt/Co/Pt films. *Phys. Rev. Lett.* **110**, 107203 (2013).
25. Kim, D.-H., Moon, K.-W., Yoo, S.-C., Min, B.-C., Shin, K.-H. & Choe, S.-B. A method for compensating the Joule-heating effects in current-induced domain wall motion. *IEEE Trans. Magn.* **49**(7), 3207–3210 (2013).
26. Haazen, P. P. J., Murè, E., Franken, J. H., Lavrijsen, R., Swagten, H. J. M. & Koopmans, B. Domain wall depinning governed by the spin Hall effect. *Nature Mater.* **12**, 299–303 (2013).
27. Emori, S. *et al.* Spin Hall torque magnetometry of Dzyaloshinskii domain walls. *Phys. Rev. B* **90**, 184427 (2014).
28. Kim, D.-Y., Kim, D.-H. & Choe, S.-B. Intrinsic asymmetry in chiral domain walls due to the Dzyaloshinskii–Moriya interaction. *Appl. Phys. Express* **9**, 053001 (2016).
29. Jung, S.-W., Kim, W., Lee, T.-D., Lee, K.-J. & Lee, H.-W. Current-induced domain wall motion in a nanowire with perpendicular magnetic anisotropy. *Appl. Phys. Lett.* **92**, 202508 (2008).
30. Je, S.-G., Yoo, S.-C., Kim, J.-S., Moon, J., Min, B.-C. & Choe S.-B. Drastic emergence of huge negative spin-transfer torque in atomically thin Co layers. arXiv:1512.03405v1 (2015).
31. Jué, E. *et al.* Chiral damping of magnetic domain walls. *Nature Mater.* **15**, 272–277 (2016).

## Acknowledgements

This work was supported by a National Research Foundations of Korea (NRF) grant that was funded by the Ministry of Science, ICT and Future Planning of Korea (MSIP) (2015R1A2A1A05001698 and 2015M3D1A1070465). D.-H.K. was supported by a grant funded by the Korean Magnetics Society. B.-C.M. was supported by the KIST institutional program and the National Research Council of Science & Technology (NST) grant (No. CAP-16-01-KIST).

## Author Contributions

D.-H.K. planned and designed the experiment and S.-B.C. supervised the study. D.-H.K. and D.-Y.K. carried out the measurement. S.-C.Y. and B.-C.M. prepared the samples. S.-B.C. and D.-H.K. performed the analysis and wrote the manuscript. All authors discussed the results and commented on the manuscript.

## Additional Information

**Competing Interests:** The authors declare no competing financial interests.

**How to cite this article:** Kim, D.-H. *et al.* Wide-Range Probing of Dzyaloshinskii–Moriya Interaction. *Sci. Rep.* **7**, 45498; doi: 10.1038/srep45498 (2017).

**Publisher's note:** Springer Nature remains neutral with regard to jurisdictional claims in published maps and institutional affiliations.



This work is licensed under a Creative Commons Attribution 4.0 International License. The images or other third party material in this article are included in the article's Creative Commons license, unless indicated otherwise in the credit line; if the material is not included under the Creative Commons license, users will need to obtain permission from the license holder to reproduce the material. To view a copy of this license, visit <http://creativecommons.org/licenses/by/4.0/>

© The Author(s) 2017